

REPORT DOCUMENTATION PAGE				<i>Form Approved</i> OMB No. 0704-0188	
Public reporting burden for this collection of information is estimated to average 1 hour per response, including the time for reviewing instructions, searching existing data sources, gathering and maintaining the data needed, and completing and reviewing this collection of information. Send comments regarding this burden estimate or any other aspect of this collection of information, including suggestions for reducing this burden to Department of Defense, Washington Headquarters Services, Directorate for Information Operations and Reports (0704-0188), 1215 Jefferson Davis Highway, Suite 1204, Arlington, VA 22202-4302. Respondents should be aware that notwithstanding any other provision of law, no person shall be subject to any penalty for failing to comply with a collection of information if it does not display a currently valid OMB control number. PLEASE DO NOT RETURN YOUR FORM TO THE ABOVE ADDRESS.					
1. REPORT DATE (DD-MM-YYYY) 5/9/2012		2. REPORT TYPE Final Report		3. DATES COVERED (From - To) June 2009 - November 2001	
4. TITLE AND SUBTITLE L1-Based Approximations of PDEs and Applications				5a. CONTRACT NUMBER FA9550-09-1-0424	
				5b. GRANT NUMBER	
				5c. PROGRAM ELEMENT NUMBER	
6. AUTHOR(S) Jean-Luc Guermond Bojan Popov				5d. PROJECT NUMBER	
				5e. TASK NUMBER	
				5f. WORK UNIT NUMBER	
7. PERFORMING ORGANIZATION NAME(S) AND ADDRESS(ES) Texas A&M University (formally Research Foundation) Office of Sponsored Research Services 400 Harvey Mitchell Pkwy S. College Station, TX 77845				8. PERFORMING ORGANIZATION REPORT NUMBER	
9. SPONSORING / MONITORING AGENCY NAME(S) AND ADDRESS(ES) AFOSR 875 N RANDOLPH ST ARLINGTON, VA 22203				10. SPONSOR/MONITOR'S ACRONYM(S)	
				11. SPONSOR/MONITOR'S REPORT NUMBER(S) AFRL-OSR-VA-TR-2012-1029	
12. DISTRIBUTION / AVAILABILITY STATEMENT DISTRIBUTION A: APPROVED FOR PUBLIC RELEASE					
13. SUPPLEMENTARY NOTES					
14. ABSTRACT					
15. SUBJECT TERMS					
16. SECURITY CLASSIFICATION OF:			17. LIMITATION OF ABSTRACT U	18. NUMBER OF PAGES 18	19a. NAME OF RESPONSIBLE PERSON
a. REPORT U	b. ABSTRACT U	c. THIS PAGE U			19b. TELEPHONE NUMBER (include area code)

Final report for grant FA9550-09-1-0424

L^1 -BASED APPROXIMATIONS OF PDES AND APPLICATIONS

Jean-Luc Guermond

Department of Mathematics Texas A&M University College Station, TX

Bojan Popov

Department of Mathematics Texas A&M University College Station, TX

1 Summary

The objective of this project was to develop robust numerical methods for solving mathematical models of nonlinear phenomena such as nonlinear conservation laws, surface/image/data reconstruction problems, advection-dominated flows, multi-phase flows, and free-boundary problems, where shocks, fronts, and contact discontinuities are driving features and pose significant difficulties for traditional numerical methods.

The main thrust of this research program was to explain some intriguing numerical observations reported by Lavery, Jiang, and Guermond [4]¹ that seemed to indicate that for some classes of PDE's equipped with non-smooth coefficients and/or non-smooth right-hand sides it pays off to approximate the solution directly in L^1 . Contrary to standard stabilized L^2 -based techniques, L^1 -based methods did not seem to require additional ad hoc tunable coefficients or limiting procedures.

We have finally elucidated some of the above issues and we can report that the major achievements of our 2.5 year long L^1 -program spanning from June 2009 to November 2011 are the following:

- (1) **L^1 -minimization for PDEs:** We have shown that it does pay off to work in L^1 for steady equations Hamilton-Jacobi equations. We have proved in particular that L^1 -based finite element approximations converge to the physically relevant solution, i.e., the so-called viscosity solutions. We have developed algorithms for solving L^1 -based discrete minimization problems and we have

¹Only the papers written by the PIs under the umbrella of the present grant are cited and listed at the end of the report in the Reference section.

proved that our algorithms converge and their computational complexity is optimal in one space dimension.

- (2) **L^1 -reconstruction of data:** We have developed algorithms for L^1 -based data fitting and surface reconstruction. We have developed a localized (easy to parallelize) version of the L^1 -based minimization methods.
- (3) **Entropy viscosity for nonlinear conservation laws:** As a by-product of the research program on the L^1 -approximation of Hamilton Jacobi equations we have discovered that time-dependent nonlinear conservation equations can be stabilized by using the so-called *entropy viscosity*.

We believe that the entropy viscosity idea is an important conceptual breakthrough. The main stabilization mechanism in this method is a nonlinear dissipation proportional to the local size of an entropy production. For this reason we call the method entropy viscosity. We propose to use the local residual of an entropy equation to construct the artificial viscosity. One immediate consequence of this choice is that the viscosity is proportional to the entropy production, which is known to be large in shocks and to be zero in contact discontinuities. As a result, this strategy automatically distinguishes shocks and contact discontinuities, i.e., no detection of contacts and no artificial compression is needed. This strategy is inspired from the observations that we made when solving Hamilton Jacobi equations using the L^1 -minimization technique: approximate L^1 -minimizers solve the PDE in the smooth regions but they do not in the non-smooth regions; the approximation mechanism is dominated completely by the entropy production in the non-smooth regions. We have implemented this idea and we have obtained very encouraging numerical results. In particular, we have observed excellent resolution of contact waves, and the additional cost of the L^1 -minimization is avoided.

2 Hamilton-Jacobi equations

2.1 One space dimension

We have introduced an L^1 -based minimization technique to solve steady Hamilton-Jacobi equations in [11]. We have proved in this paper that the method converges to the unique viscosity solution. Adding an entropy penalty to the L^1 functional is critical to achieve convergence to the correct solution.

We have also proposed an algorithm of optimal complexity to solve one-dimensional steady Hamilton-Jacobi equations in [13] and [6]. We have proved

convergence in the case of one-dimensional stationary Hamilton-Jacobi equations with convex Hamiltonian. Actually we have proved in one space dimension that our algorithm is quite similar to the well-known Fast marching/Fast sweeping methods of Sethian and Osher which means that the Fast marching/Fast sweeping methods construct almost minimizers in L^1 . This property was totally unknown. We conjecture that this analogy still holds in higher space dimensions. If true our methodology would then prove convergence of the Fast marching/Fast sweeping algorithms, since we have already proved that sequences of almost L^1 -minimizers converge to the viscosity solution of the equation.

We show in Figure 1 the solution of

$$\frac{1}{2\pi}|u'(x)| - |\cos(2\pi x)| = 0, \quad u(0) = 0, \quad u(1) = 0, \quad (1)$$

using the algorithm developed in [13] and [6].

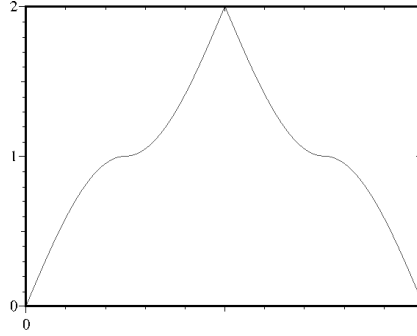


Figure 1: Solution to (1) using 100 degrees of freedom.

2.2 Higher-space dimensions

We have revisited the one-dimensional theory developed in [11] and extended it to higher-space dimensions in [12]. We introduce an L^1 -functional augmented with an entropy functional that is dimension-dependent. We have proved in [12] that the approximate solution obtained by minimizing this combined functional converges to the unique viscosity solution.

The method has been tested numerically. We show in Figure 2 two computations performed on the eikonal equation using two types of meshes. The first mesh is aligned with the discontinuities of the gradient of the solution and the second mesh is unstructured. The results are reported in Figure 2. For both mesh types, we observe that the approximate L^1 -minimizer is similar to the Lagrange

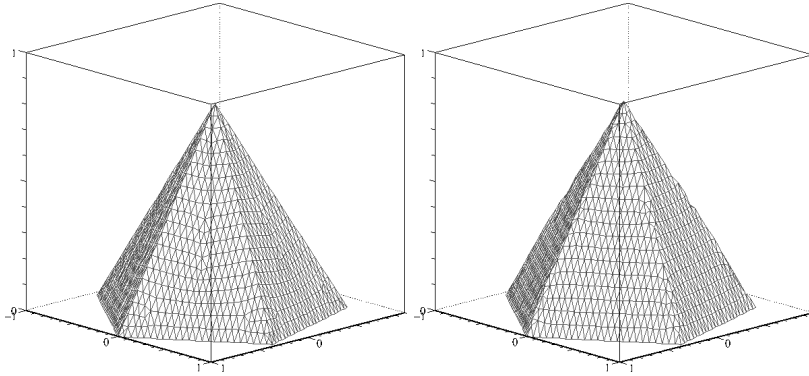


Figure 2: Pentagon: Aligned unstructured mesh (left); Non-aligned unstructured mesh (right).

interpolant of the exact solution on the same mesh. This is what we should expect intuitively: i.e., the L^1 -minimization process solves the equation in the region where the solution is smooth and simply ignores the PDE in the regions where the gradient of the exact solution is discontinuous.

3 Surface and image reconstruction

3.1 L^1 data reconstruction

In geometric modeling and image reconstruction, one often tries to *extract* a shape or recover a piece-wise smooth surface from a set of measurements. That is, one wants to find a surface that satisfies constraints or fits given data and is visually pleasing. The objectives could vary with the applications but the intuitive goal is to preserve the *shape* of the object. For example, one may want to reconstruct a convex body if the underlying data comes from a convex object, a flat surface if the data is locally flat, or preserve a particular structure of the level sets. Sometimes, this type of problem is solved by minimizing an L^2 -norm of the Hessian.

In [15, 3], we have taken a different approach that we think is well suited for man-made surfaces, Digital Elevation Models (DEM), and enhancement of digital images. Namely, we minimize the total variation of the gradient of a function constructed on a finite element space satisfying interpolatory constraints. Minimizing the total variation of the gradient of a smooth function amounts to minimizing the L^1 -norm of its second derivatives. The key observation is that using the L^1 -

norm in the minimization process produces oscillation free surfaces. In [15, 3] we have developed a surface reconstruction technique based on the minimization of the total variation of the gradient. Convergence of the method is established and an interior point algorithm solving the associated linear programming problem is introduced. The reconstruction algorithm is illustrated on various test cases including natural and urban terrain data, and enhancement of low-resolution or aliased images.

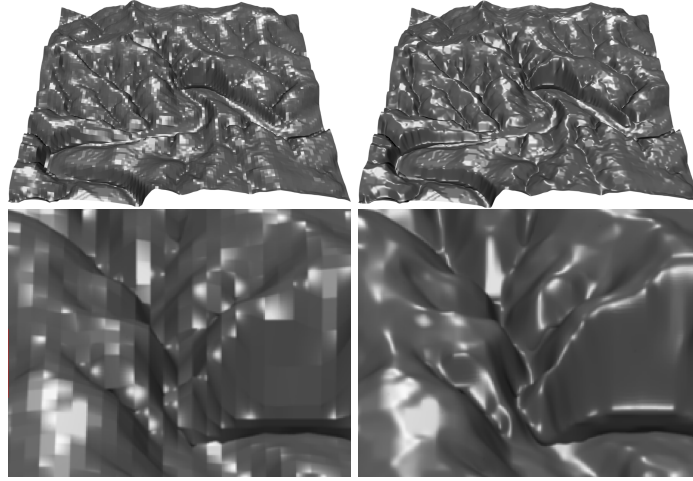


Figure 3: Barton Creek data set. \mathbb{Q}_1 interpolant (top left); L^1 -reconstruction (top right); zoom of the \mathbb{Q}_1 interpolant (bottom left); zoom of the L^1 -reconstruction (bottom right).

In Figure 3 we reconstruct the elevation map of an area near Barton Creek in Austin, Texas. We use the elevation map of a $3\text{km} \times 3\text{km}$ terrain. The data comes from the Digital Elevation Models (DEM) data files produced by the U.S. Geological Survey (USGS) (DEM data is available at <http://www.webgis.com/terraindata.html>). The data set is sampled on 100×100 uniform Cartesian mesh. The \mathbb{Q}_1 interpolant of the data and the L^1 cubic reconstruction are shown in Figure 3 (two top panels). To better appreciate the quality of the L^1 cubic reconstruction we show a zoom of a small region in the two bottom panels of Figure 3.

In Figure 4 we show how the L^1 reconstruction technique can help to reconstruct blurred or aliased text. The original aliased picture is in the top panel of Figure 4. It is the word CESKOSLOVENSKO. The left panel in the second and third row are zooms of the original picture. In the second row the image is in gray scale and in the third row we use only black and white. The center and right pan-

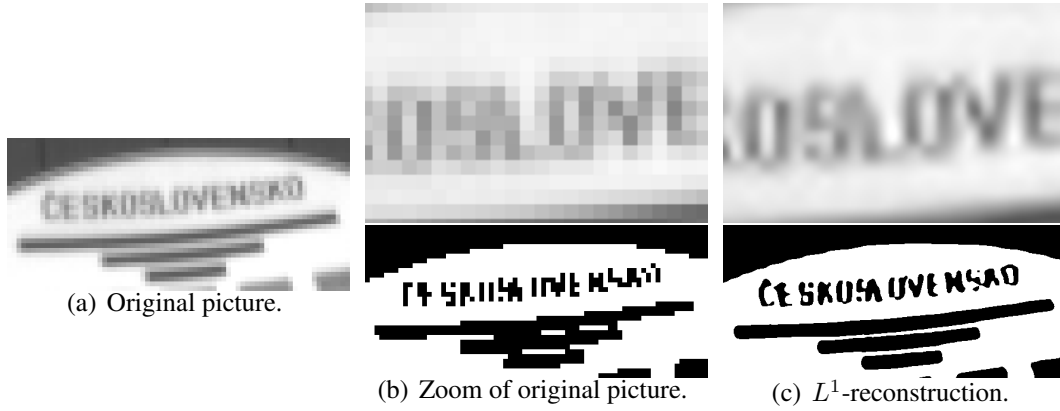


Figure 4: ČESKOSLOVENSKO test case. Original picture (left column). Zoom of original picture (middle column, gray image (top), BW thresholding (bottom)). L^1 -reconstruction (right column, gray image (top), BW thresholding (bottom))

els are two different cubic L^1 reconstructions. It is clear that our technique really improves the image since one can certainly read the aliased word in the picture in the bottom right panel.

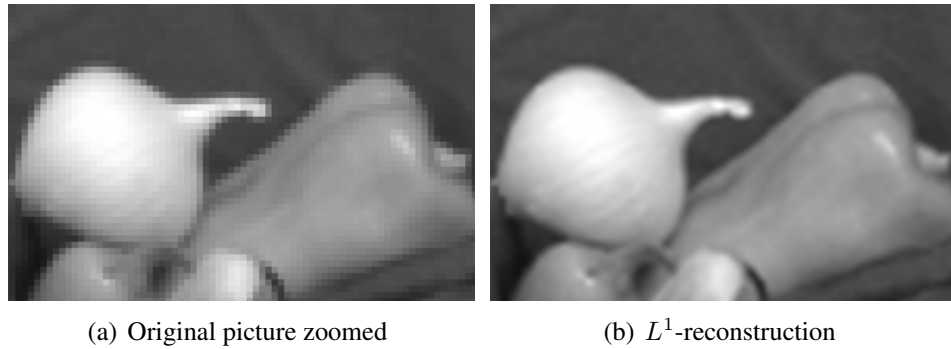


Figure 5: Pepper test case.

We now show how our L^1 -reconstruction method works on a pepper image. A zoom of original down-sampled image is shown in the left panel in Figure 5. The result obtained using the L^1 -reconstruction is shown in the right panel in Figure 5. The improvement is clear again.

3.2 Local L^1 -minimization and parallelization

The key question one faces when using L^1 -minimization techniques is to make the minimization algorithm fast and capable of solving very large problems. We have considered two possible approaches: (i) local L^1 -minimization, which allows parallel implementation; (ii) different implementation method (i.e., augmented Lagrangian algorithm). Both of these were implemented for image/surface enhancement and linear transport problems.



Figure 6: Lena Test. Original image (top left); down-sampled image (top center); Standard bi-cubic reconstruction (top right); First Jacobi iteration of local L^1 -reconstruction (bottom left); Third Jacobi iteration (bottom center); Global L^1 -reconstruction (bottom right);.

In our previous works the L^1 -minimization problems were formulated globally over the whole domain of interest, see [2, 3] and even though the results obtained are excellent, the computational time are too large for large problems. To address this issue we have developed a new method based on a divide-and-conquer strategy. Instead of computing the minimizer over the whole domain at once, we divide the domain of interest into sub-domains and compute local L^1

minimizers in each sub-domain. This local L^1 minimizing technique is used in a Jacobi iterative scheme to reach the global minimizer. The Jacobi iterations are repeated until a residual is within a fixed tolerance. The construction of the local L^1 minimization problems is not trivial and it is not evident that by performing local minimizations one can reach the global L^1 -minimizer. Our numerical results confirms that this is true in all the test cases that we have considered so far.

Figure 6 shows results for the standard Lena test problem. We have down-sampled the 512×512 gray-scale original image to a 128×128 image by averaging 4×4 pixel blocks, and then the down-sampled image is reconstructed with both the local and the global L^1 minimization algorithm. The improvement over the standard bi-cubic algorithm used in practice is clear. These tests reveal that 1) local solutions on aggregates are faster than solving the global problem; 2) only a few (in many cases just one) Jacobi iterations are enough to be close to the global L^1 -minimizer for practical purpose. This technique can used for designing fast algorithms for surface reconstruction and transport equations with *sparse* local structures/residuals. Our numerical tests show that the local algorithm performs well on the Digital Elevation Models that we considered in [2, 3].

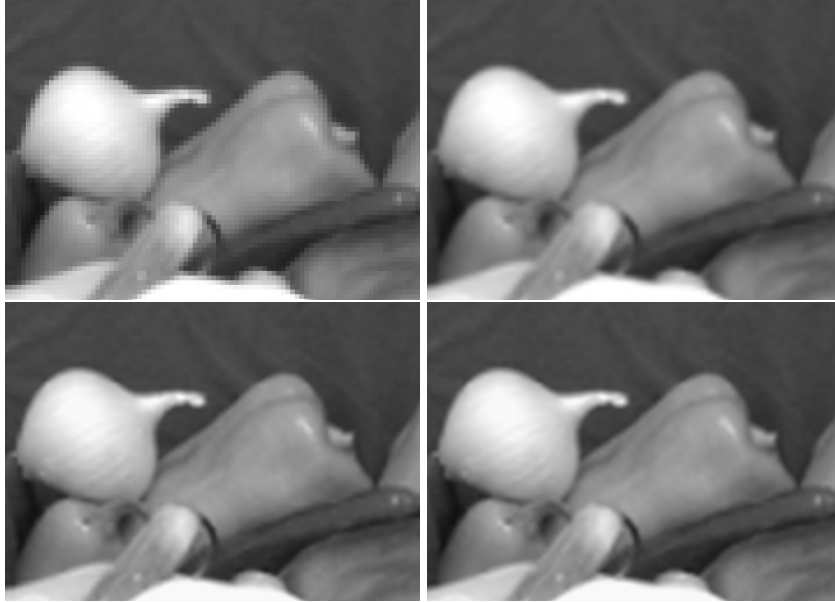


Figure 7: Pepper test. Down-sampled image (top left); standard Bi-cubic reconstruction (top right); First Jacobi iteration of local L^1 -reconstruction (bottom left); global L^1 -reconstruction (bottom right);.

The local L^1 minimization algorithm can be implemented in parallel. In a parallel setting the local sub-problems are solved concurrently, and the final result is communicated between CPUs afterwards. Table 1 shows the speed-up obtained on a machine with 64 processors for the Lena and the pepper tests. Note that these speed up figures are conservative, as we obtain them by performing a few more Jacobi iterations than one typically needs in practice.

<i>Problem</i>	Global algorithm	Local parallel algorithm	Speed up
Lenna test	2300 s	56 s	41
The pepper test	1741 s	21 s	83

Table 1: CPU time for the global and local parallel algorithms (64 CPUs).

Another direction of improvement is to use a different algorithm than the interior point method for computing the L^1 minimizers. We have explored an operator splitting technique known as the Augmented Lagrangian algorithm. We have been able to show that, depending on the accuracy required, the Augmented Lagrangian can be faster. Table 2 compares performance of the two algorithms on the pepper image problem for different accuracy requirements, see Figure 7.

<i>tolerance</i>	0.5	0.2	0.1	0.01	0.001
Augmented Lagrangian Algorithm	51	185	612	4250	10000+
Interior Point Method	173	284	519	1741	8872

Table 2: Time required to reach the same error tolerance for the Interior point and the Augmented Lagrangian algorithm. Times are in seconds.

Our numerical tests show that the augmented Lagrangian method converges relatively fast initially but then slows down. The interior point is slow but superior when it comes to achieve high accuracy. We are currently working on combining the fast, but inaccurate, Augmented Lagrangian method and the slow, but accurate, Interior Point method into an adaptive algorithm. The above results will be reported in a forthcoming paper [14].

4 Entropy viscosity

We report in this section on our findings regarding approximation of nonlinear conservation equations using a new method that we call entropy viscosity.

4.1 Entropy viscosity for nonlinear scalar conservation laws

Nonlinear conservation equations can all be put into the following general form:

$$\partial_t u(x, t) + \nabla \cdot f(u(x, t)) = 0, \quad x \in \Omega, \quad t > 0, \quad (2)$$

with $u|_{t=0} = u_0$ and appropriate boundary conditions. The scalar initial boundary value problem has a unique entropy solution which satisfies an additional set of differential inequalities

$$\partial_t E(u) + \nabla \cdot F(u) \leq 0, \quad (3)$$

for any pairs $E(u)$ and $F(u)$ such that E is convex and $F'(u) = E'(u)f'(u)$. The function E is called entropy and F is the associated entropy flux. For convex fluxes (i.e., if f is convex) in one space dimension it is known that one entropy pair, for example the one generated by $E(u) = \frac{1}{2}u^2$, is enough to select the unique entropy solution. Physical systems have at least one entropy pair and the entropy inequality (3) is the mathematical form of the second principle of thermodynamics. It is expected that the auxiliary inequality (3) serves as a selection criteria and guarantees convergence of the numerical approximation to the correct *physical solution* of the nonlinear system. Therefore, it is desirable (and necessary) to somehow incorporate the entropy dissipation (3) in a numerical scheme.

A traditional way of selecting the entropy solution of (2) consists of adding viscous dissipation

$$\partial_t u^\epsilon + \nabla \cdot f(u^\epsilon) - \nabla \cdot (\epsilon \nabla u^\epsilon) = 0, \quad (4)$$

where $\epsilon > 0$ and it can be shown in general that $u^\epsilon \rightarrow u$ when $\epsilon \rightarrow 0$. The parameter ϵ is usually taken to be proportional to the local mesh size when constructing numerical approximation of (4) and this limits the convergence rate to first-order at most. The use of artificial viscosity to solve nonlinear conservation equations has been pioneered by Neumann and Richtmyer and popularized later by Smagorinsky for LES purposes and by Ladyženskaja for theoretical purposes in the analysis of the Navier-Stokes equations. The early versions of artificial viscosities being overly dissipative, the interest for these technique has faded over the years, especially in the Discontinuous Galerkin Finite and Finite Volume literature, where up-winding and limiters have been shown to be efficient and to yield high-order accuracy. Up to a few exceptions slope limiting is a one-dimensional concept that does not easily generalize to unstructured meshes in higher dimensions. Moreover, the theoretical understanding of the stability and convergence of limiters is currently restricted to uniform grids and scalar equations in one space

dimension. For the above reasons and, among other things, the fact that artificial viscosities are easy to implement, the interest for artificial viscosity has lately been revived in the DG literature and in the Continuous Galerkin (CG) literature as well.

We have introduced a new technique for generating high-order numerical approximations for nonlinear conservation equations in [9, 5, 10] using continuous finite elements and spectral elements. The main stabilization mechanism in this method is a nonlinear dissipation proportional to the local size of an entropy production. For this reason the method is called entropy viscosity. It is usually argued in the literature that good artificial viscosities can be computed from measures of the local regularity of the solution or from the local residual of the PDE. We propose to take a slightly different route by considering the local residual of an entropy equation to construct the artificial viscosity.

$$\epsilon \sim ch^2 |\partial_t E(u) + \nabla \cdot F(u)|. \quad (5)$$

One immediate consequence of this choice is that the viscosity is proportional to the entropy production, which is known to be large in shocks and to be zero in contact discontinuities. As a result, this strategy makes an automatic distinction between shocks and contact discontinuities, and this subtle distinction cannot be made by any of the two classes of methods mentioned above. We also think that using the residual of the conservation equation may be less robust than using the entropy residual. This argument is based on the observation that consistency requires the residual of the PDE to converge to zero in the distribution sense as the mesh-size goes to zero, whereas the very nature of entropy implies that the entropy residual converges to a Dirac measure supported in the shocks. This implies that the entropy residual focuses far better in shocks than the PDE residual, and it is in this sense that we claim that the PDE residual is less reliable than the entropy residual. This can be better understood by considering the simple case of the one-dimensional Burgers equation $\partial_t u + \frac{1}{2} \partial_x u^2 = 0$ with initial data $u(x, 0) = 1$ if $x < 0$ and $u(x, 0) = 0$ otherwise. The entropy solution is $u(x, t) = 1 - H(x - \frac{1}{2}t)$ where H the Heaviside function. One observes that the residual of the equation is zero, whereas the entropy residual is an negative measure: $\frac{1}{2} \partial_t u^2 + \frac{1}{3} \partial_x u^3 = -\frac{1}{12} \delta(x - \frac{1}{2}t)$, where δ is the Dirac measure. This effect is very well illustrated on the one-dimensional Burgers equation over the interval $(0, 1)$ with initial data $\sin(\pi x)$, see Figure 8. We show in this figure the entropy viscosity computed by using either the quadratic entropy $E(u) = \frac{1}{2} u^2$ (first and second panel from the left) or $E(u) = u$ (third and fourth panels). Choosing $E(u) = u$ corresponds to using the residual of the PDE for the viscosity. These tests show that choosing

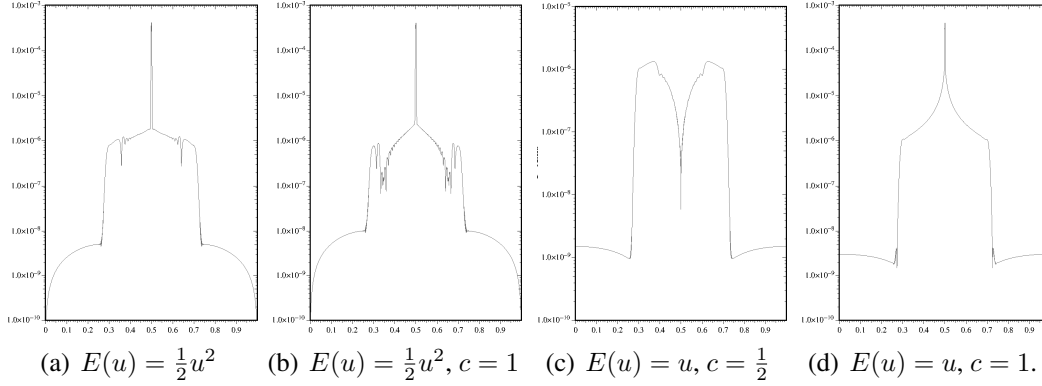


Figure 8: Entropy viscosity in log scale for the Burgers equation at $t = 0.25$

$E(u) = \frac{1}{2}u^2$ leads to better focusing of the viscosity and is more robust with respect to the multiplier c (see definition (5)).

Although no convergence proof of the entropy viscosity method has been produced yet, the method has been shown in [9, 5, 10] to deliver high-order accuracy by testing it on a large variety of benchmark problems. We have recently proved that the algorithm with explicit time stepping is indeed L^2 -stable for nonlinear scalar conservation equations, [1].

4.2 Compressible fluid dynamics

We have generalized the entropy viscosity concept to the compressible Euler equations by using the physical entropy to construct the entropy viscosity.

4.2.1 Continuous finite elements

We have tested the method with continuous finite elements. We show in Figure 9 the density field at $t = 2.86$ and the viscosity field at $t = 4$ for the classical wind tunnel problem with a forward facing step at Mach 3. We observe that the viscosity focuses very well and there is almost no viscosity in the contact discontinuity that develops at the top of the flow.

We show in Figure 10 the density field at $t = 0.2$ for the double Mach reflection problem at Mach 10. We observe again that there is almost no viscosity in the contact discontinuity that develops from the first triple point; moreover the jet develops the standard instability at the bottom of the domain.

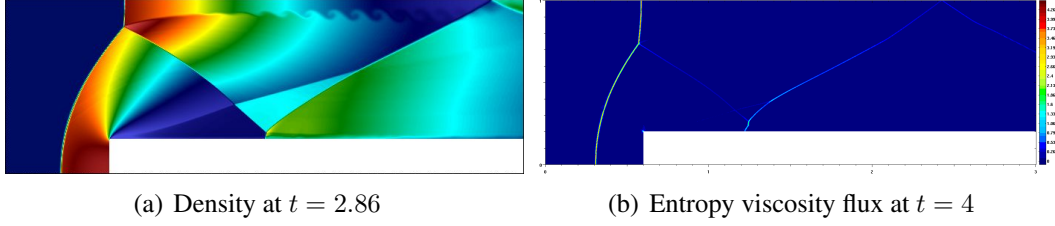


Figure 9: Wind tunnel with a step at Mach 3, \mathbb{P}_1 approximation.

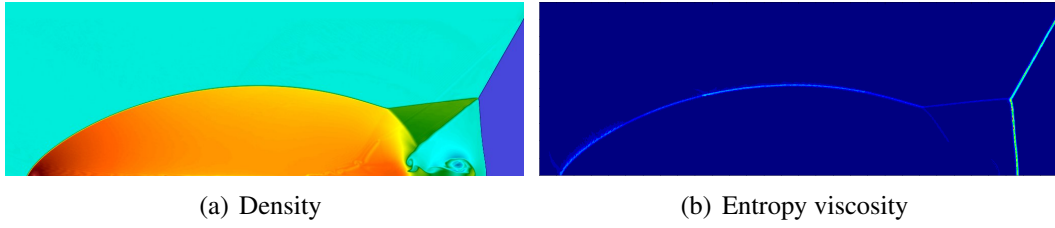


Figure 10: Double Mach reflection, $t = 0.2$, \mathbb{P}_1 approximation.

We have also developed two different techniques to enforce boundary conditions on curved boundaries, which is not an easy task for nonlinear conservation equations. We are also using the entropy viscosity framework to construct a goal oriented refinement strategy. The method is well developed by now, see [10, 7, 8]. We have solved various benchmark problems with finite elements, spectral elements and Fourier. We show typical results in Figure 11.

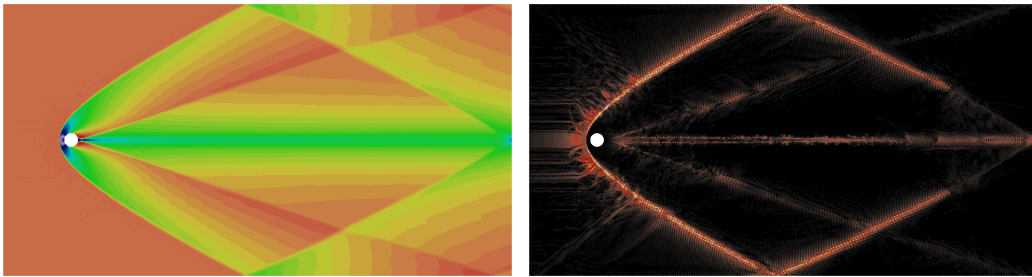


Figure 11: Supersonic around a cylinder in a tunnel. \mathbb{P}_1 approximation. Density field (left) and entropy viscosity (right).

4.2.2 Discontinuous Galerkin finite elements

The entropy viscosity method has been extended to the Discontinuous Galerkin setting in [16]. In introducing appropriate numerical fluxes the method is proved to be consistent with an entropy inequality. The numerical performance of the method is observed to be independent of the chosen polynomial degree of approximation. To the best of knowledge the extension of the entropy viscosity method to discontinuous finite elements had never been done before.

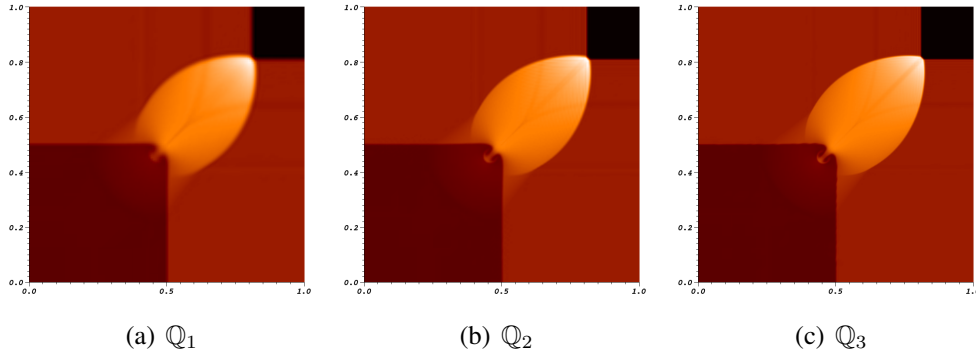


Figure 12: Riemann problem 12 at $T = 0.2$ using discontinuous Galerkin plus entropy viscosity stabilization. \mathbb{Q}_1 (left), \mathbb{Q}_2 (center), \mathbb{Q}_3 (right), 128×128 cells.

As an illustration of the method we demonstrate its performance in Figure 12 on the classical Riemann Problem 12 from a paper by Liska and Wendroff. It is a two-dimensional Riemann problem developing complex structures involving shocks and contacts. The computational domain is $\Omega = (0, 1)^2$. The heat capacity ratio is $\gamma = 1.4$ and the initial data is

$$\begin{aligned} p &= 1, & \rho &= 4/5, & \mathbf{u} &= (0, 0) & 0 < x < 1/2, & 0 < y < 1/2, \\ p &= 1, & \rho &= 1, & \mathbf{u} &= (3/\sqrt{17}, 0) & 0 < x < 1/2, & 1/2 < y < 1, \\ p &= 1, & \rho &= 1, & \mathbf{u} &= (0, 3/\sqrt{17}), & 1/2 < x < 1, & 0 < y < 1/2, \\ p &= 2/5, & \rho &= 17/32, & \mathbf{u} &= (0, 0), & 1/2 < x < 1, & 0.5 < y < 1. \end{aligned} \quad (6)$$

Due to the finite speed of propagation of perturbations, the solution of the problem in $(0, 1)^2$ is identical to the restriction to $(0, 1)^2$ of the solution to the Riemann problem in \mathbb{R}^2 up to time $t^* := \frac{s}{2(s^2+0.6)} > 0.32$, where $s = \frac{3}{\sqrt{17}}$. The time stepping is done with RK4 with CFL = 0.25. The computations are done with \mathbb{Q}_1 , \mathbb{Q}_2 and \mathbb{Q}_3 discontinuous finite elements on a grid composed of $16384 = 128^2$

quadrangular cells. The total number of scalar degrees of freedom for the \mathbb{Q}_1 , \mathbb{Q}_2 and \mathbb{Q}_3 approximations are 65536, 146456, 262144, respectively, i.e., $4^7 \times (k + 1)$.

We show in Figure 12 the density field at $T = 0.2 < T^*$ for the \mathbb{Q}_1 , \mathbb{Q}_2 and \mathbb{Q}_3 approximations. The results compare well with reference solutions. The shocks and the fine structures that develop behind them are very well described. The method behaves well as the polynomial degree of the approximation increases.

4.3 Lagrangian hydrodynamics

Through collaborations with colleagues at Lawrence Livermore National Laboratory, we have recently started to extend the entropy viscosity methodology to Lagrangian hydrodynamics. Our first experiments have shown that the method extends naturally to this setting without any particular difficulty, thereby proving again that the methodology that we propose is very flexible. This is an ongoing work, no formal report has yet been written, but we can show some preliminary computations done by a student that has been supported by the grant (V. Tomov).

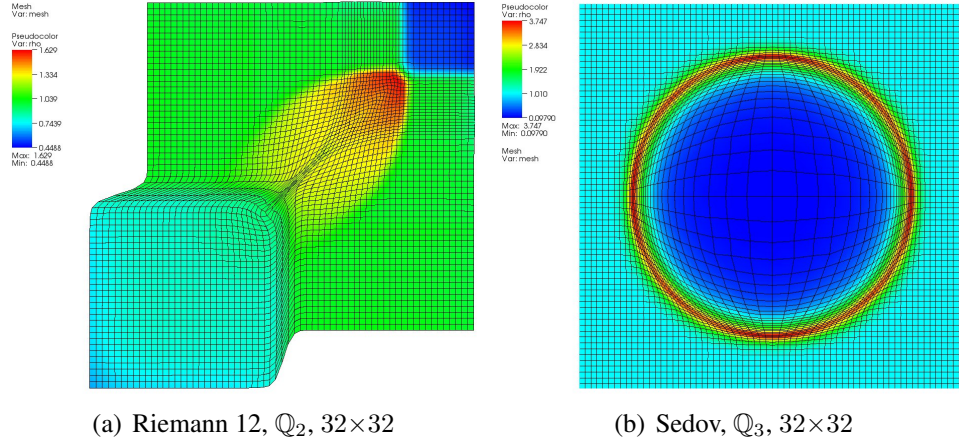


Figure 13:

We show in the left panel of Figure 13 the solution of the Riemann 12 problem at $t = 0.2$. The deformation of the Lagrangian mesh is clearly visible. This computation has been done with \mathbb{Q}_2 continuous finite elements. We show in the right panel of Figure 13 the solution of the so-called Sedov blast problem. Here again the deformation of the Lagrangian mesh is clearly visible. This computation has been done with \mathbb{Q}_3 continuous finite elements.

Acknowledgment/Disclaimer

This work was sponsored (in part) by the Air Force Office of Scientific Research, USAF, under grant/contract number FA9550-09-1-0424. The views and conclusions contained herein are those of the authors and should not be interpreted as necessarily representing the official policies or endorsements, either expressed or implied, of the Air Force Office of Scientific Research or the U.S. government.

Personnel Supported During Duration of Grant

Jean-Luc Guermond, Professor, Texas A&M University.

Bojan Popov, Professor, Texas A&M University.

Murtazo Nazarov, Visiting Assistant Professor, Texas A&M University.

Habiballah Talavatifard, Graduate student, Texas A&M University.

Vladimir Tomov, Graduate student, Texas A&M University.

References

- [1] A. Bonito, J.-L. Guermond, and B. Popov. Stability analysis of explicit entropy viscosity methods for non-linear scalar conservation equations. *Math. Comp.*, 2012. In review.
- [2] V. Dobrev, J.-L. Guermond, and B. Popov. *Surface reconstruction via L^1 -minimization.*, pages 32–43. Berlin: Springer, 2009.
- [3] V. Dobrev, J.-L. Guermond, and B. Popov. Surface reconstruction and image enhancement via L^1 -minimization. *SIAM J. Sci. Comput.*, 32(3):1591–1616, 2010.
- [4] J. L. Guermond. A finite element technique for solving first-order PDEs in L^p . *SIAM J. Numer. Anal.*, 42(2):714–737, 2004.
- [5] J.-L. Guermond. On the use of the notion of suitable weak solutions in CFD. *Int. J. Numer. Methods Fluids*, 57:1153–1170, 2008.
- [6] J.-L. Guermond, F. Marpeau, and B. Popov. A fast algorithm for solving first order 1D PDEs by L^1 -minimization. *Communications in Mathematical Sciences*, 6(1):199–216, 2008.

- [7] J.-L. Guermond, M. Nazarov, and B. Popov. Implementation of the entropy viscosity method. *submitted*, 2011.
- [8] J.-L. Guermond, M. Nazarov, and B. Popov. A posteriori error estimations for compressible euler equations using entropy viscosity. *submitted*, 2011.
- [9] J.-L. Guermond and R. Pasquetti. Entropy-based nonlinear viscosity for fourier approximations of conservation laws. *C. R. Math. Acad. Sci. Paris*, 346:801–806, 2008.
- [10] J.-L. Guermond, R. Pasquetti, and B. Popov. Entropy viscosity method for nonlinear conservation laws. *Journal of Computational Physics*, 230:4248–4267, 2011.
- [11] J.-L. Guermond and B. Popov. L^1 -minimization methods for Hamilton-Jacobi equations: The one-dimensional case. *Numer. Math.*, 109:269–284, 2008.
- [12] J.-L. Guermond and B. Popov. L^1 -minimization methods for Hamilton-Jacobi equations. *SIAM J. Numer. Anal.*, 47:339–362, 2008/09.
- [13] J.-L. Guermond and B. Popov. An optimal L^1 -minimization algorithm for stationary Hamilton-Jacobi equations. *Commun. Math. Sci.*, 7(1):211–238, 2009.
- [14] J.-L. Guermond, H. Talavatifard, and B. Popov. Parallel L^1 -minimization. 2012. preprint.
- [15] B. P. V. Dobrev, J.-L. Guermond. Surface reconstruction via l_1 -minimization. In *NAA 2008*, volume 5434 of *LNCS*. Springer Berlin/Heidelberg, 2009.
- [16] V. Zingan, J.-L. Guermond, J. Morel, and B. Popov. Implementation of the entropy viscosity method with the discontinuous galerkin method. *Comput. Methods Appl. Mech. Engrg.*, 2012. in press.